NO MAJOR CHANGES ON PALEOCLIMATE AND PALEOENVIRONMENT ACROSS THE EOCENE–OLIGOCENE TRANSITION IN THE CENTRAL ROCKY MOUNTAINS

by

SARA AYYASH

Presented to the Faculty of the Graduate School of

The University of Texas at Arlington in Partial Fulfillment

of the Requirements

for the Degree of

MASTER OF SCIENCE IN EARTH AND ENVIRONMENTAL SCIENCE

THE UNIVERSITY OF TEXAS AT ARLINGTON

December 2015

Acknowledgements

I would like to express my gratitude to those who assisted me over the course of this project. A huge thank-you to my advisor Dr. Majie Fan for her extreme patience during my graduate studies and guidance on this project. She has helped me learn the material, conduct research and interpret data. This thesis would not have been possible without her help. I would also like to extend my appreciation to my committee member Dr. Griffith for her help and guidance, and committee member Dr. Arne Winguth for his advices, guidance, and article references.

I would like to thank Dr. Hawkins for his assistance and advice on the statistical analyses of my data. I would also like to thank my friends for their support, and other graduate students in Dr. Fan's research group for their help and constant encouragement and the group lunch time.

Lastly, I appreciate my family for their constant support even though they question what I work on frequently and had to put up with my books and papers spread-out everywhere. I would like to thank both my parents Ahmad Ismail Ayyash and Ibtisam Ahmad Ayyash for constantly encouraging me to continue my studies and also sending me articles about geology in every couple of weeks.

November 24, 2015

Abstract

NO MAJOR CHANGES ON PALEOCLIMATE AND PALEOENVIRONMENT ACROSS THE EOCENE–OLIGOCENE TRANSITION IN THE CENTRAL ROCKY MOUNTAINS

Sara Ayyash, M.S.

The University of Texas at Arlington, 2015

Supervising Professor: Majie Fan

Earth's climate has experienced dramatic cooling during the Eocene-Oligocene Transition (EOT) based on well-constrained marine geological records, however, a consensus on the terrestrial responses to this event has not been reached. The White River Formation in the central Rocky Mountains, western U.S.A., is a well-dated stratigraphic unit covering the EOT. The formation contains tuffaceous mudrock and sandstone that were deposited in fluvial and eolian depositional environments. Here I study oxygen isotope ratios and clumped isotope temperatures of carbonate cements and bulk organic carbon isotope ratios in order to reconstruct the paleoenvironment and paleoclimate across the EOT. These carbonate cements were formed as low-Mg calcite in equilibrium with unevaporated surface water during early diagenesis based on XRD results, low Mg/Ca and Sr/Ca ratios, and petrographic observations, thus the isotope compositions reflect near-surface climate and environmental conditions. My results show that clumped isotope temperature and organic carbon $\delta^{13}C$ values remained stable across the EOT. The carbonate $\delta^{18}O$ and calculated water $\delta^{18}O$ values both increase 0.5 ‰ after the EOT, which I interpret as a result of gradual drying during the middle Cenozoic. My results show that the paleoclimate and paleoenvironment in the central

Rocky Mountains did not experience major changes across the EOT. I suggest that high topography in the central Rocky Mountains prior to the global cooling event may have buffered local responses to global cooling.

Table of Contents

List of Illustrations

List of Tables

Chapter 1

Introduction

1.1 Objectives

Earth's climate has undergone a dramatic shift from its "greenhouse" state to its "icehouse" form during the Eocene-Oligocene Transition (EOT) (e.g., Zachos et al., 2001). This cooling event has been well constrained and studied in marine geological record because of reliable biostratigraphic and magnetostratigraphic controls, The cooling event presents itself in different forms in marine record, including the increase of calcium carbonate content and benthic foraminifera $\delta^{18}O$ and $\delta^{13}C$ values and Mg/Ca ratios, which are resulted from the deepening of the calcite compensation depth associated with the decrease of atmospheric carbon dioxide concentration across the EOT (e.g., Van Andel and Moore, 1974; Van Andel, 1975; Zachos et al., 1996; Lear et al., 2000; Coxall et al., 2005), the increase of planktonic foraminifera $\delta^{18}O$ and $\delta^{13}C$ values, alkenone unsaturation and TetraEther indices resulted from cooling of ocean surface water (e.g., Keigwin, 1980; Liu et al., 2009; Wade et al., 2012), and marine species turnover (e.g., Sydney et al., 1984; Audrey, 1992; Squires, 2003; Dunkley Jones et al., 2008; Aubry and Bord, 2009).

The temperature drop occurred very rapidly, within ~300 kyr across the EOT and is documented as the Oi-1 event that represent major glaciation of Antarctic. (Zachos et al., 1996; Liu et al., 2009). Oi-1 is marked as the initiation of Antarctica ice-sheets, triggered by the drop in temperature during the Cenozoic. The documented temperature drop is ~4.5-12 °C for deep seawater (Kennett, 1977; Lear et al., 2000, Zachos et al., 2001), and at least 3°C for surface seawater (Lear et al., 2008; Liu et al., 2009; Wade et al., 2012). Two major mechanisms have been proposed to explain the rapid cooling, including decreasing atmospheric CO_2 concentration by enhanced silicate weathering (e.g., Raymo and Ruddiman, 1992; Broecker and Sanyal, 1998; DeConto et al., 2003; Liu et al., 2009; Pearson et al., 2009, Goldner et al., 2014), which was associated with increases of ocean productivity and carbon burial (e.g., Zachos at al., 1996; Zachos and Kump, 2005), and opening the Tasman Gateway and Drake Passage, which caused development of a circum-Antarctic current and changes in ocean circulation (e.g., Mikolajewicz

et., 1993; Diester-Haass and Zahn, 1996; Ivany et al., 2008; Sijp et al., 2009, Goldner et al., 2014). Both mechanisms may be associated with the change of Earth's orbital configuration (Zachos et al., 2001).

Although much research has been conducted to understand how terrestrial climate responded to the EOT cooling, well-constrained terrestrial records are relatively rare, and available data show heterogeneous responses. Climate and environmental responses reconstructed from terrestrial records include a drop of mean annual temperature of 3-13 °C (Wolfe, 1994; Retallack et al., 2007; Zanazzi et al., 2007; Schouten et al., 2008; Hren et al., 2013), increased seasonality with cooler winter but stable or warmer summer temperature (Wolfe, 1994; Gimes et al., 2005; Eldrett et al., 2009), aridification of continental interior (Retallack et al., 1983; Terry et al., 2001; Retallack et al., 2007; Cather et al., 2008; Dupont-Nivet et al., 2008; Kraatz and Geisler, 2010; Abels et al., 2011), land snails, lizard, and mammalian fauna turnover (e.g., Evanoff et al., 1992; Augé and Smith, 2009; Kraatz and Geisler, 2010). Several of these records are constructed from western U.S.A. However, other studies have suggested climate and land mammal fauna in western U.S.A. were stable across the EOT (Prothero and Heaton, 1995; Kohn et al., 2004; Strömberg, 2004; Sheldon et al., 2009), which raises ambiguity of terrestrial responses to the cooling.

The White River Formation and its equivalent of the White River Group distributed in North Dakota, South Dakota, Montana, Nebraska, Colorado, and Wyoming are of latest Eocene-early Oligocene age (e.g., Terry, 2001; Retallack, 2007). These strata should preserve critical information of terrestrial climatic and environmental responses of EOT in continental interior. Currently, most of the studies to the White River Formation/Group are focused on examining paleosol geomorphology and geochemistry, phytolith assemblages, and stable isotope composition of mammal tooth enamel and bones in Toadstool Park and Badlands National Park in northwestern Nebraska and southwestern South Dakota (Retallack et al., 1983; Terry et al., 2001; Strömberg, 2004; Retallack et al., 2007; Zanazzi et al., 2007; Zanazzi and Kohn, 2008; Boardman and Secord 2013). These studies provide contrasting results and interpretation of paleoclimate and paleoenvironment in the western interior during the EOT. Specifically, the

aridification and temperature decline recorded in paleosol geomorphology and geochemistry studies and oxygen isotope compositions of mammal fossil tooth and bones (Retallack et al., 1983; Terry et al., 2001; Retallack et al., 2007; Zanazzi et al., 2007; Zanazzi and Kohn, 2008) are not presented in the change of phytolith assemblages and oxygen isotope compositions of fossil tooth of more diverse fossil faunas (Strömberg, 2004; Boardman and Secord, 2013). Therefore, additional research is needed to further understand the terrestrial climatic and environmental responses of EOT in the continental interior of western U.S.A.

The White River Formation near Douglas, eastern Wyoming, is one of the best-preserved units with reliable North American Land Mammal ages and radiometric ages (Figure 1-1) (Evanoff et al., 1992; Evanoff and Larson, 1998; Prothero and Whittlesey, 1998). In this thesis, I reconstruct the paleoclimate and paleoenvironment in eastern Wyoming by integrating oxygen and clumped isotope compositions and Mg/Ca and Sr/Ca ratios of carbonate cements, and bulk organic carbon isotope compositions. Results collected from this project provide an additional archive to aid in understanding how continental climate and environment responded to the EOT cooling.

1.2 Geological Setting and Stratigraphy

The Laramide orogeny occurring during the late Cretaceous to the early Eocene, formed several Precambrian basement-cored uplifts and intervening sedimentary basins in Wyoming (Dickinson et al., 1988). The region also experienced uplift and associated erosion during the late middle Eocene, possibly due to thermal uplift related to asthenosphere upwelling (Cather et al. 2012; Fan et al., 2014). During the middle and late Cenozoic, widespread volcanic activity occurred in the western U.S.A. and provide large amount of ash to the study area (Lipman et al., 1972).

The White River Formation near Douglas, Wyoming is about 230 m thick, and is composed of conglomerate, and tuffaceous mudrock and sandstone that were deposited in fluvial and eolian depositional environments (Figure 1-2) (Evanoff et al., 1992). At least eight tuff beds of 50-110 cm thick present in the Formation, and the beds can be traced throughout the region (Evanoff, 1990). The Formation is divided into the Chadron and Brule members by a thick white

tuff bed known as tuff 5 (Evanoff et al., 1992). The Chadron Member is composed of interlayered green/brown clayey mudstone, nodular brownish tan sandy mudstone, and thin beds of sandstone, with several thick sandstone ribbons (Evanoff, 1990; Evanoff et al., 1992).

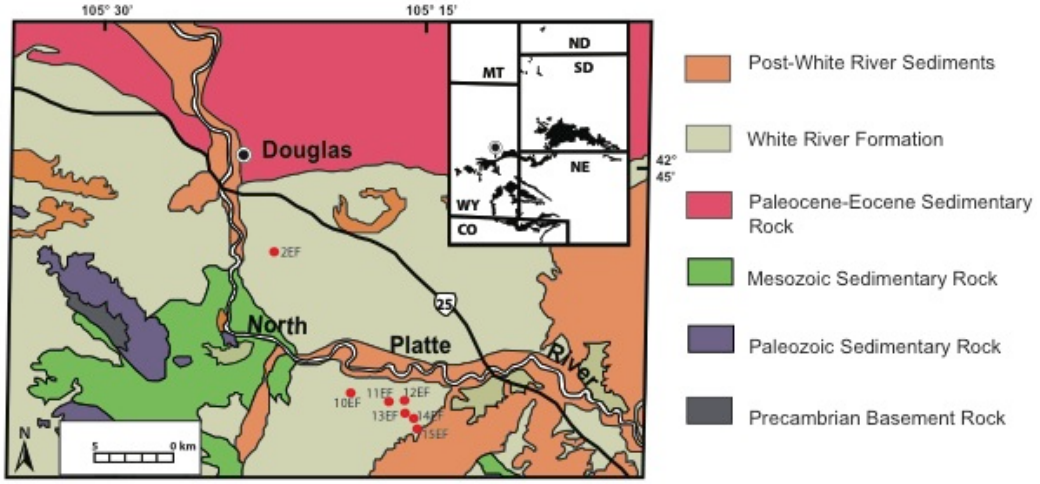

Figure 1-1 Geologic map of the study area in eastern Wyoming. Red dots represent the locations of the sampled stratigraphic sections following Evanoff (1990). Black area in figure insert represent outcrops of the White River Formation. Modified from Evanoff (1990) and Terry (2001).

The Brule Member is composed of brownish tan sandy mudstone and massive tan sandy siltstones with a few ribbons of sandstone and conglomerate sandstone (Evanoff, 1990; Evanoff et al., 1992). Evanoff et al., (1992) suggests fluvial depositional environment in the Chadron and lower Brule members grades into eolian dryland loess depositional environment in the upper Brule Member. Evanoff (1990) suggests that the tuff beds in the Chadron Member were altered to opal-Ct, clinoptilolite or smectite, whereas the tuff beds in the Brule Member are glass rich.

Radiometric age constraints of the Formation were based on biotite K-Ar, sanidine or biotite 40Ar/39Ar, and zircon U-Pb dating of the tuff beds. Biotite 40Ar/39Ar dating places tuff 3 at 34.48 ± 0.08 Ma (Swisher and Prothero 1990; Terry, 2001). Biotite and Sanidine 40Ar/39Ar dating place tuff 5 at 33.91 ± 0.06 Ma, and 33.59 ± 0.02 Ma, respectively (Swisher and Prothero 1990; Obradovich et al., 1995), and zircon U-Pb dating places tuff 5 at 34.0 ± 0.2 Ma (Scott, 2000). Thus tuff 5 is roughly at the Eocene-Oligocene boundary (Figure 1-2). Tuff 7, which is stratigraphically above tuff 5, was dated as 30.7 ± 0.6 Ma based on biotite 40Ar/39Ar dating and 32.9 ± 0.2 Ma based on zircon U-Pb dating (Scott, 2000). The 40Ar/39Ar ages are younger than

U-Pb ages, which may be caused by argon loss. Here I use the zircon U-Pb ages as the depositional ages. Ages for individual samples were assigned based on linear extrapolation of sedimentation rate derived from dated tuff 3, 5 and 7.

1.3 Modern Climate

Current climate in eastern Wyoming is semiarid with an annual precipitation amount of ~ 43 cm. This area is influenced by Westerlies, tropical air masses from the Gulf of Mexico, and air masses from the Arctic, Pacific, and Atlantic oceans (Bryson and Hare, 1974). Summer monsoon brings 80% of the annual precipitation from the Gulf of Mexico and Atlantic and the remaining 20% of precipitation are transported from the high-latitude Pacific by the Westerlies during the cold season (Ingraham and Taylor, 1991; Bryson and Hare, 1974). Due to cooler condensation temperatures and variations of vapor sources, winter precipitation $\delta^{18}O$ values are significantly lower, and span a larger range of values than summer precipitation $\delta^{18}O$ values (Liu et al., 2010).

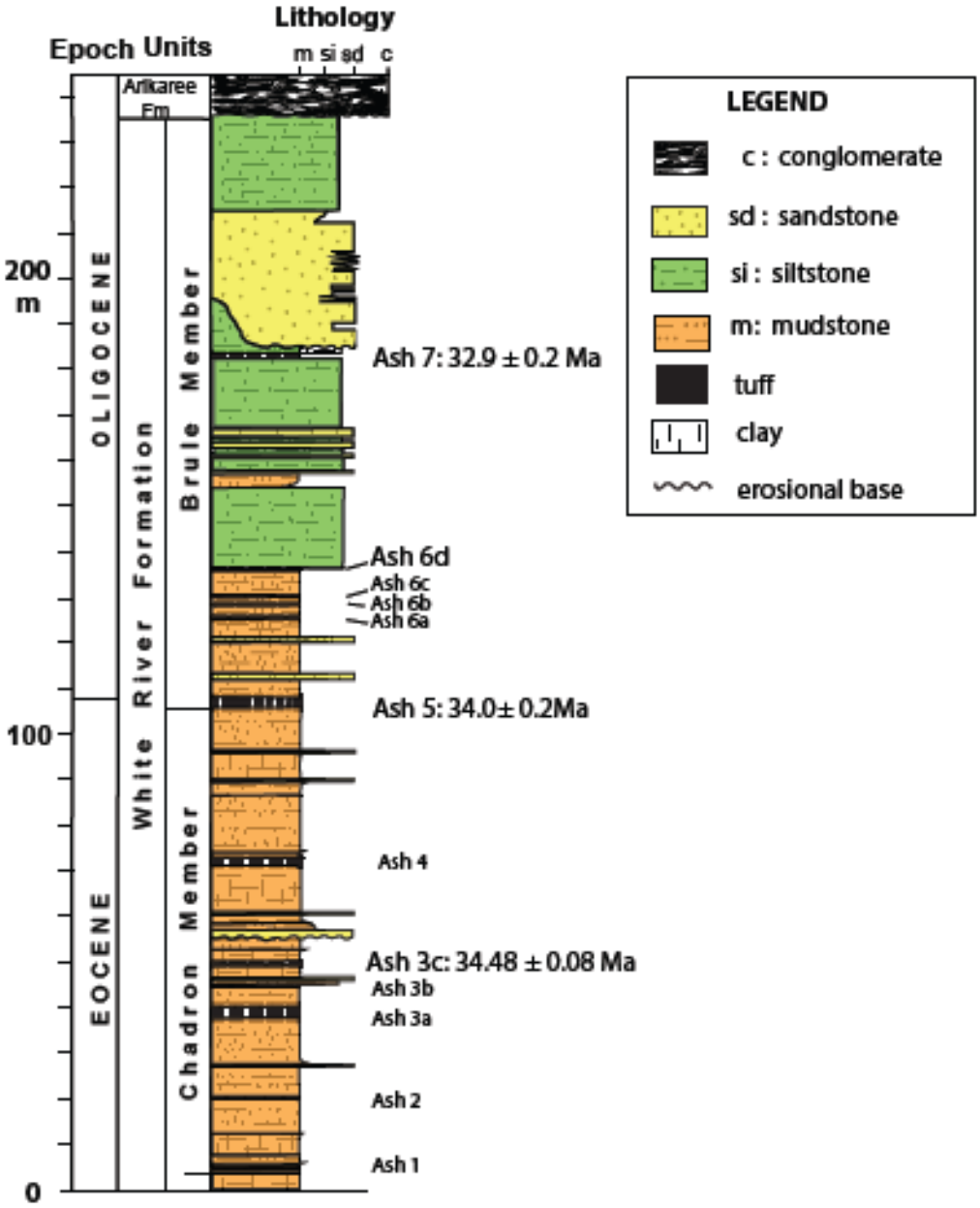

Figure 1-2 Composite stratigraphic section of the White River Formation near Douglas. Modified from Evanoff (1990).

Chapter 2

Methods

2.1 Petrographic and XRD Analysis

Evanoff (1990) described 15 individual sections of the White River Formation near Douglas, Wyoming. Samples used in this study were collected from section 2 and sections 10-15, with the EOT occurring in sections 2, 13, and 14 (Evanoff, 1990). Six samples were examined using cathodoluminescence (CL) and polarizing microscopes to evaluate diagenesis of carbonate cement. The six samples were ground using a ceramic mortar and pestle and the carbonate mineralogy was determined using X-ray diffraction (XRD) analysis.

Cathodoluminescence study of polished thin sections was carried out at Baylor University Cathodoluminescene Imaging Laboratory using a Reliotron Cathodoluminescence connected to a Nikon Digital Sight DS-U3. The instrument was operated at 7-9 kV and 0.3-.5 mA. Thin sections were also examined under a Leica polarizing microscope to characterize the fabrics of carbonate cement. Spar percentages were determined by using software Image J. Areas of spar were outlined using a tracing tool in the software. Area percentage of spar was calculated as the ratio of spar area and whole thin section area. Weight percentage of spar was then calculated by multiplying area percentage of spar and carbonate content. XRD patterns were obtained using a Bruker D8 Advance Diffractometer operated at 40 keV and 40 mA. Samples were scanned from 20° to 50° 2θ at 0.02° steps. Carbonate mineralogy were determined based on the position of the d(104) peak (Whipkey, 2002; Harris et al., 2007).

2.2 Element Ratio Analysis

Samples used for element ratio analysis were ground using a ceramic mortar and pestle. Tools were thoroughly cleaned after each sample using distilled water to minimize

cross contamination. Mg/Ca and Sr/Ca ratios of 11 representative samples were analyzed to evaluate the influence of evaporation on carbonate isotope compositions (Appendix A). Inductively coupled plasma-atomic emission spectroscopy (ICP-AES) was used to analyze Sr/Ca and Mg/Ca ratios of the representative samples. Approximately 25 mg of each sample was digested in 4 mL of 10% ultra-pure acetic acid in acid cleaned centrifuge tubes until reaction was complete (i.e., no more bubbles). These centrifuge tubes were cleaned using 10% ultra-pure nitric acid. Samples were then centrifuged at 3000 RPM for 10 minutes. The liquid was separated from the solid and 0.5 mL of the liquid was diluted in 5 mL of 10% trace metal clean nitric acid. The dissolved Ca, Mg, and Sr were measured at wavelengths of 220.9, 285.2 and 421.6 nm respectively. Multiple standard mixtures were prepared with concentrations ranging from 1.00 to 200.00 ppm for Ca, 0.25 to 50.00 ppm for Mg, and 0.01 to 2.00 ppm for Sr. Additionally two blanks were prepared using the same method. The method detection limit for Ca, Mg and Sr was calculated following Zhang (2007) after measuring a dilute standard (n = 7) to be better than 120 µg/L, 2 µg/L, and 1 µg/L respectively. Precision was calculated by using the relative standard deviation of multiple analysis of sample EF12-27 (n = 3) and found to be better than 1.0%, 2.0%, and 0.2% for Ca, Mg and Sr respectively. The analytical precision for Sr/Ca and Mg/Ca ratios is better than 1%.

2.3 Clumped Isotolope Geochemistry Analysis

Clumped isotope compositions of five representative samples were studied to understand the formation temperature of the carbonate cements (Appendix A). Carbonate clumped isotope thermometry uses the temperature-dependent enrichment of $^{13}C^{18}O^{16}O$ isotopologues with respect to a stochastic distribution to determine carbonate mineralization temperature (Ghosh et al., 2006; Passey et al., 2010). The definition of clumped isotope ratios (Δ_{47}) and its relationship to temperature are described in Appendix

B. Clumped isotope temperature enables the calculation of water $\delta^{18}O$ values without estimating temperature. Carbonate clumped isotope analysis was conducted at Johns Hopkins University following the methods of Passey et al. (2010). Two or three aliquots of each sample were reacted at 90°C with 100% phosphoric acid, with the resultant CO_2 being cryogenically purified before analysis on a Thermo MAT 253 mass spectrometer. Equilibrium CO_2 samples prepared at 1000 °C and 30 °C were analyzed concurrently with the sample unknowns to normalize sample Δ_{47} values. Clumped isotope data of calcite cements are reported relative to the absolute reference frame (ARF) of Dennis et al. (2011), and temperatures are calculated using the composite calibration for CO_2 extraction at 75-100 ºC in Defliese et al. (2015).

During the course of the study, two internal carbonate standards (Carrara Marble and 102-GC-AZ01) and one international carbonate standard (NBS-19) were analyzed multiple times. The mean Δ_{47} values and standard deviation (SD) of these standards are 0.399 ± 0.013 ‰ (n = 10), 0.713 ± 0.016 ‰ (n = 14), and 0.391 ± 0.010 ‰ (n = 3), respectively. The standard errors (SE) for Δ_{47} reported in Table 2 are calculated as SE = SD/√N, where SD is the observed standard deviation for repeated analyses of samples, and N is the number of repeated analyses. If the observed SD is lower than the known laboratory precision (0.013 ‰), which is the mean precision we observed for repeated analyses of standards, SE is calculated using SD = 0.013‰. Error in T(Δ_{47}) is calculated by propagating the SE for Δ_{47} and an estimated error in Δ_{47} of 0.0028 ‰ for the acid temperature correction (Passey et al., 2010), through the paleotemperature equation in Defliese et al. (2015).

2.4 Stable Isotope Geochemsity Analysis

Samples used for isotope ratio analysis were examined under magnification to avoid sampling visible spar, and powdered samples were collected using a hand-held drill

or ground using a ceramic mortar and pestle. Tools were thoroughly cleaned after each sample using distilled water to minimize cross contamination. A total of 101 samples were studied for cement carbonate $\delta^{13}C$ and $\delta^{18}O$ values, and a total of 92 samples were studied for carbonate content, total organic carbon (TOC), and $\delta^{13}C_{org}$ values (Appendix A). Isotope ratios of carbon and oxygen are used to interpret changes in paleoenvironment and paleoclimate. Oxygen isotope ratios in carbonate are a function of temperature and the water the carbonate precipitated in, while carbon isotope ratios are a function of biogenic sources, atmospheric CO_2 and additional inorganic carbon. The isotope ratios are expressed in delta notation defined in appendix B.

Analyses of stable isotope ratios, carbonate percentage, and TOC were conducted in the Light Stable Isotope Laboratory at the University of Texas at Arlington. One set of samples for TOC and bulk $\delta^{13}C_{org}$ values analysis were placed in centrifuge tubes and reacted with 10% of hydrochloric acid for at least 72 hours to remove carbonate. Samples were then washed with DI water to neutral pH. All the test tubes containing samples were placed on a high-speed vortex for a few minutes to ensure a full wash then were centrifuged for 15 minutes and decanted. Wet samples were placed in an oven at 40°C for a week until completely dried. Sample weight loss after the acid pretreatment was used to calculate carbonate percentage. The same samples were also processed using acid fumigation method to remove carbonate. Samples were weighed into silver capsules and were moistened with one drop of DI water. Sample were then placed in a sealed container and exposed to 100 ml of fuming hydrochloric acid for 4 days and dried at 40 °C for 3 days. Dried samples were quickly packed in tin capsules before analysis.

TOC and bulk $\delta^{13}C_{org}$ values were analyzed using a Costech elemental analyzer connected to a Thermo Finnigan Delta-V Advantage isotopic ratio mass spectrometer

(IRMS) via Conflo IV device. The raw TOC data were corrected for carbonate percentage. Carbonate $\delta^{13}C$ and $\delta^{18}O$ values were analyzed using a Gasbench connected to the Delta-V Advantage IRMS. All Isotope values are reported in δ notation relative to PeeDee Belemnite (PDB). Ancient water $\delta^{18}O$ values were calculated based on the fractionation equation of Kim and O'Neil (1997) and the average temperature of the five clumped isotope temperatures. The precisions of all isotope values are better than 0.1 ‰ based on repeated analysis of USGS 40, USGS 41, NBS18 and NBS19. The the precision of TOC is better than 0.3%.

Power-spectral analyses of isotope data were preformed in order to determine the orbital cycles in my isotope data using the MATLAB code of Dorothee (2014).

Chapter 3

Results

3.1 Petrographic and XRD Analysis

Under polarizing petrographic microscope, the carbonate cements are dominantly micritic with isolated vugs filled by spar (Figure 3-1). The spar carbonate of the six representative samples range from 0.13% to 4.72%. Examinations under cathodoluminescence show that the micritic carbonate cement exhibits predominantly dull luminescence with isolated, intermixed bright specks of orange luminescence, and the spar filling vugs are bright orange and display zoning (Figures 3-2 C, D). XRD results of the six representative samples show that the carbonate cements are low-magnesium calcite (Figure 3-2).

3.2 Element Ratios

Element concentration data are summarized in Table A-1. Ca concentration ranges from 58 to 144 mg/L. Mg and Sr concentrations are low, ranging from 18 to 910 µg/L and 35 to 78 µg/L, respectively. Sr/Ca ratio ranges from 0.17 to 0.31 mmol/mol, and Mg/Ca ratio ranges from 0.3 to 10.0 mmol/mol. All results are higher than the detection limits of the instruments.

3.3 Clumped Isotope Geochemistry

Clumped isotope data are summarized in Table A-2. Temperatures calculated from the Δ_{47} values range from 19 °C to 30 °C, with an average of 24 °C. T-test results show that the T(Δ_{47}) values are not statistically different before and after the EOT (d.f.=4; x^2=7.78; P=0.10) (Figure 3-5). The temperature of an altered snail is 35 °C, slightly higher than the other five samples. Calculated water $\delta^{18}O$ values of the five samples range from -8.4 ‰ to -10.1 ‰.

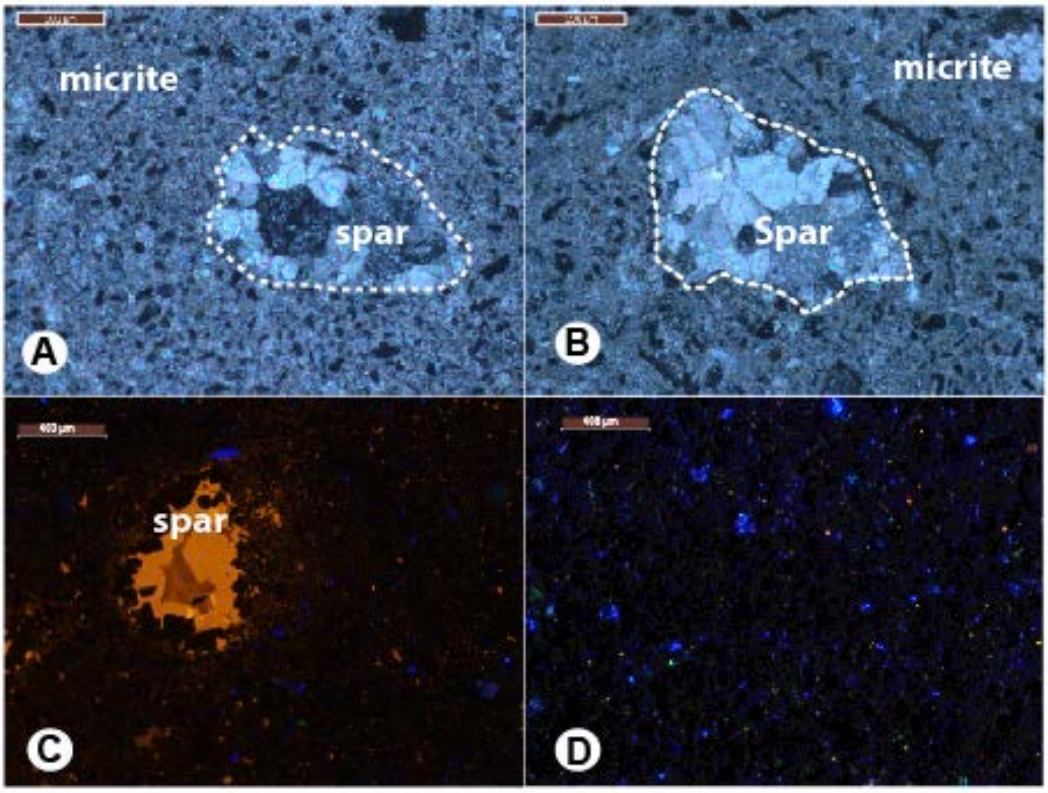

Figure 3-1 Photographs of representative thin sections of the White River Formation, (A) and (B) are under cross-polarized light showing micritic texture of cement, and spar-filled vugs. Note the low abundance of grains and high abundance of carbonate cement. Grains are predominantly quartz and volcanic glass. Scale bars are at 200 µm. (C) CL image showing bright orange luminescence and zonation of a spar-filled vug, and micritic cement in dull luminescence with minor flakes of orange luminescence. (D) CL image showing dull luminescence. Blue luminescence represents quartz grain. Scale bars are at 400 µm.

3.4 Stable Isotope Geochemistry

Stable isotope data are summarized in Table A-2. TOC% of all samples are less than 0.3% and carbonate percentage ranges from 4.2% to 62.7%. Bulk $\delta^{13}C_{org}$ values of samples pretreated using acid digestion method vary between -33.9 ‰ and -25.5 ‰, with an average of -28.5 ‰. Bulk $\delta^{13}C_{org}$ values of samples pretreated using acid fumigation

method vary between -29.0 ‰ and -25.1 ‰, with an average of -27.3 ‰. The $\delta^{13}C_{org}$ values of samples pretreated using acid digestion method is more variable than the $\delta^{13}C_{org}$ values of the same samples pretreated using acid fumigation method, and there is no linear correlation between the two groups of data (Figure 3-4). Carbonate $\delta^{18}O$ values vary from -10.6 ‰ to -19.8 ‰, with an average of -11.9 ‰ (Figure 3-3). By assuming the carbonate formation temperature remained stable at 24°C, the calculated water $\delta^{18}O$ values range from -8.4‰ to -11.4‰ (VSMOW). In box and whisker plots, the mean carbonate $\delta^{18}O$ value increases ~0.5 ‰ (d.f.=58; x^2= 79.08 ; P=0.005), and the mean calculated water $\delta^{18}O$ value also increases ~0.5 ‰ across the EOT (d.f.=58; x^2=91.95; P=0.0005) (Figure 3-5).

Spectral analyses of isotope data allow for the identification of cyclicities, particularly the Milankovitch orbital cycles. Carbonate oxygen and carbon isotope data and calculated water oxygen isotope data display cycles of ~167 kyr above 95% confidence interval (Figure 3-6). However, the cycle does not present in organic carbon isotope data.

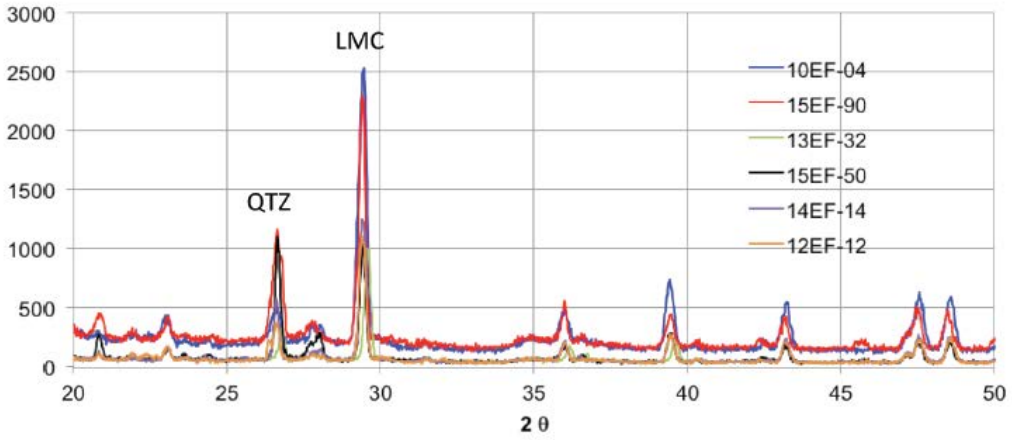

Figure 3-2 X-Ray diffraction (XRD) patterns of six representative samples from the White River Formation. Mineral indicated are quartz (QTZ) and low-magnesium calcite (LMC).

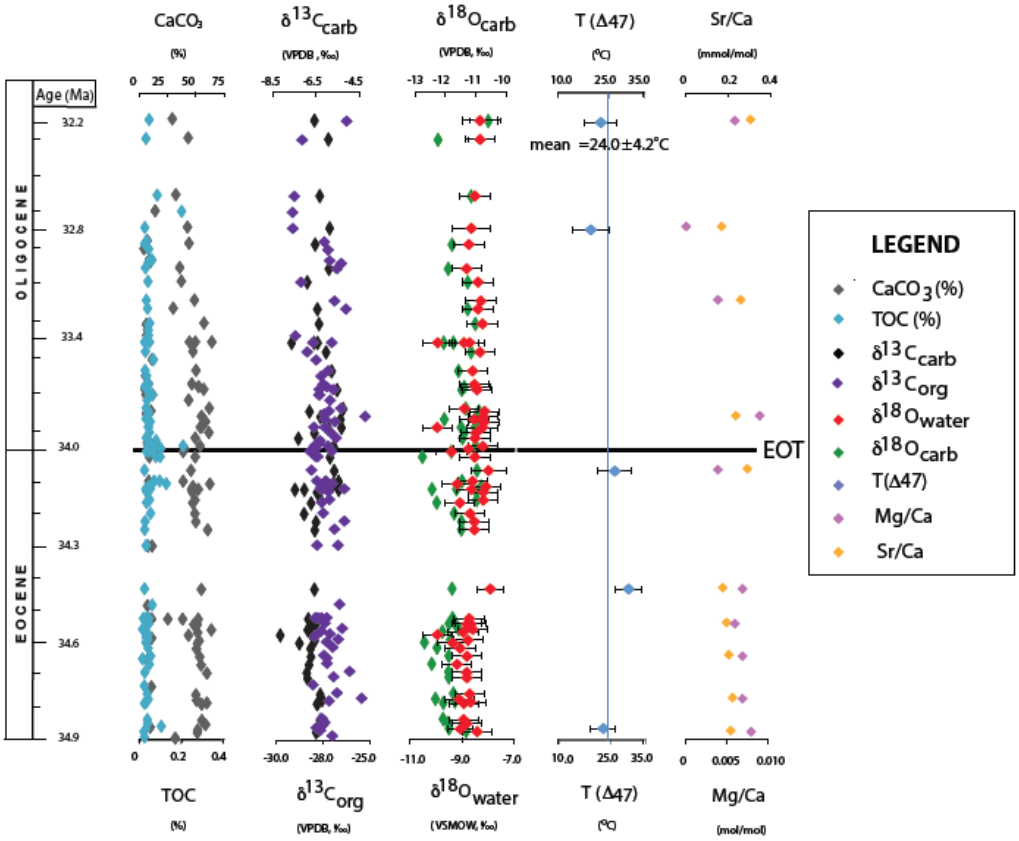

Figure 3-3 TOC, carbonate percentage, Mg/Ca and Sr/Ca ratios, and all the isotope data in this study. EOT is the Eocene-Oligocene Transition, which occurred at 34.0 Ma.

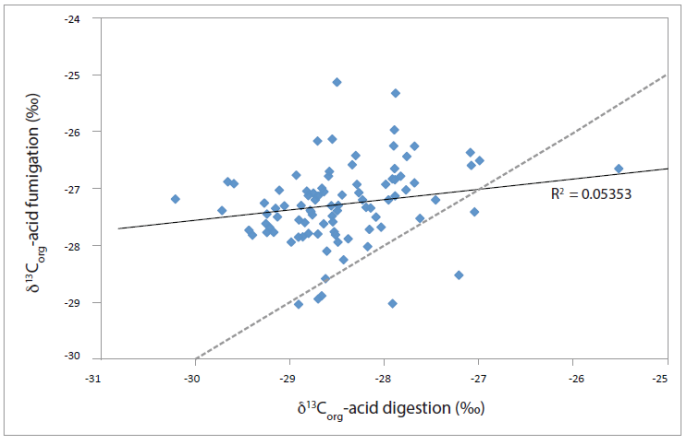

Figure 3-4 Comparison of the $\delta^{13}C_{org}$ values of samples processed using acid digestion method and acid fumigation method. The dashed line represents 1:1 line.

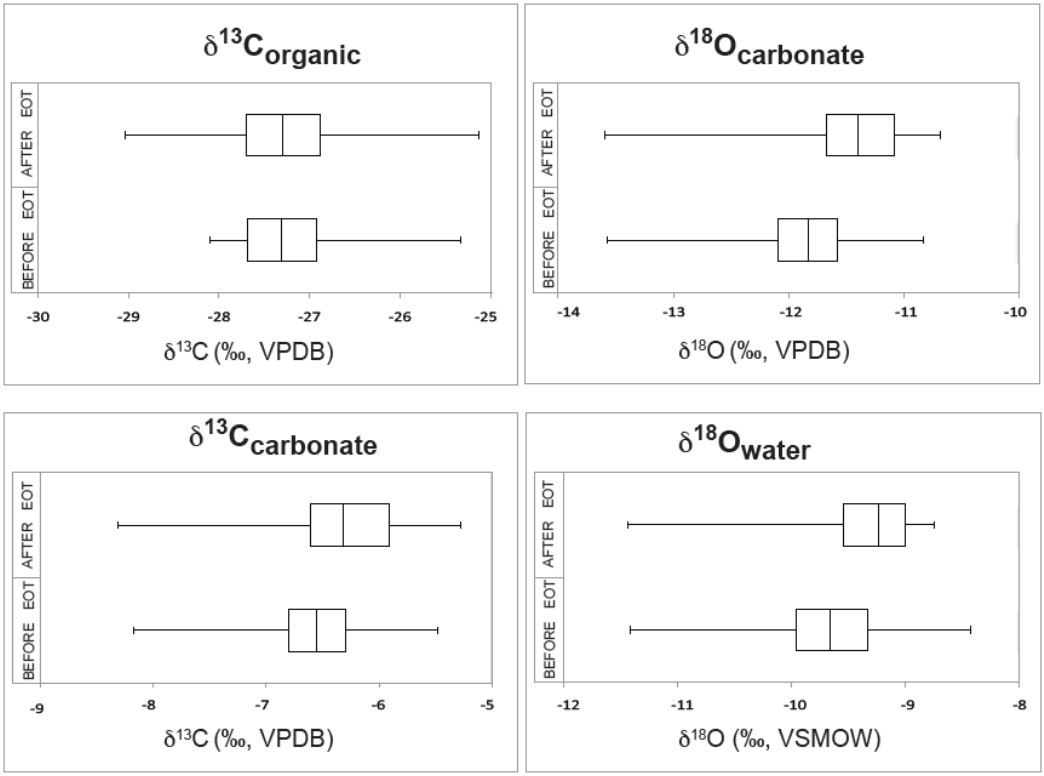

Figure 3-5 Box and whisker plots of isotope data before and after the EOT. Edges of the box represent the quartile, the vertical lines inside boxes represent the median values, and the whiskers denote the lower and upper extremes.

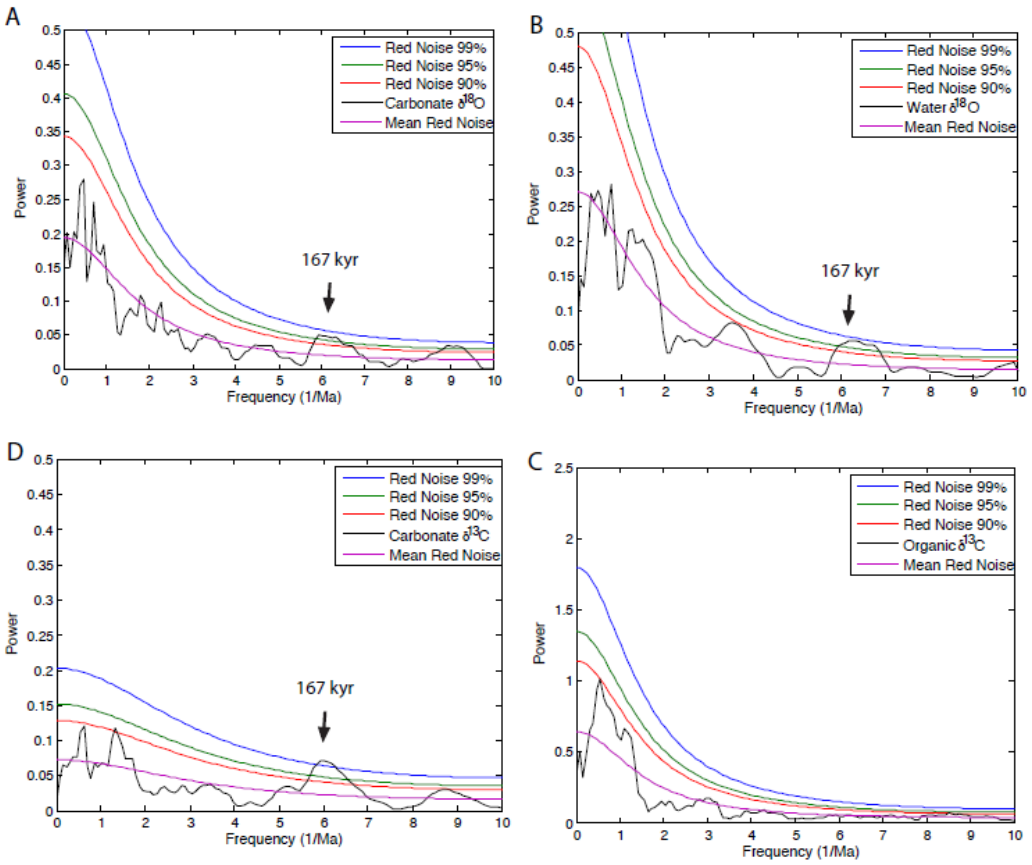

Figure 3-6 MTM Power Spectrum analyses of stable isotope data with red noise confidence intervals. (A) carbonate $\delta^{18}O$ values, (B) water $\delta^{18}O$ values, (C) carbonate $\delta^{13}C$ values, and (D) bulk organic matter $\delta^{13}C$ values using acid fumigation method.

Chapter 4

Discussion

4.1 Screening for Carbonate Diagenesis

Diagenesis of carbonate samples must be evaluated before applying stable isotope geochemistry to reconstruct paleoclimate and paleoenvironment. Carbonate cement in the White River Formation in Douglas may have experienced certain degree of diagenesis, because the petrographic results of representative samples show spar-filled vugs. Diagenesis of carbonate cement can occur during three different stages, and are classified as early, deep burial and late diagenesis (Worden and Burley, 2003). Early diagenesis takes place at near surface condition, thus the isotopic signatures of carbonate cement record near-surface climate and temperature conditions. Deep burial diagenesis takes place at high pressure and temperature, and the isotopic signatures are influence by deep formation water. Late diagenesis occurs during the recent uplift and exhumation, and the isotope signatures reflect recent climate and temperate conditions (Worden and Burley, 2003).

Two lines of evidence suggest that the micritic carbonate, which is the predominant component of the carbonate cement, was formed during early diagenesis. First, the weight percentages of cement of the representative samples are as high as 52 %. The high percentages indicate that the intergranular volumes of the samples are similar to or higher than the average original porosity of general sandstone, which is ~40 % (Sclater and Christie, 1980), suggesting the cementation was formed before compaction. Second, absent of overgrowth, partial dissolution of quartz grains, and alteration of mica and feldspar to clay minerals suggest that samples did not experience extreme pressure and temperature (Morad et al., 1994), further ruling out deep diagenesis. Although sparry carbonate may be a result of deep and late diagenesis, the

altered snail sample in the White River Formation, with 100 % sparry carbonate, has a $T(\Delta_{47})$ value that is not different from the other samples containing small amount of spars, suggesting the carbonate spar was not formed in deep and late diagenesis. Because dense micritic fabric is characteristic of vadose zone cement, and phreatic cement includes blocky spar filling isolated vugs (Wright and Tucker, 1991; Beckner and Mozley, 1998), I suggest the micritic carbonate cement in my samples was formed in vadose zone and the sparry carbonate cement was formed in phreatic zone. Although it is possible that a portion of the carbonate cement was formed during deep and late diagenesis, the percentage should be small and the influence on clumped isotope and stable isotope compositions is negligible.

Formation of carbonate cement in both vadose and phreatic zones was further supported by cathodoluminescence study to polished thin sections. Cathodoluminescence intensity is generally controlled by Mn^{2+} and several rare earth metals that act as activators and cause orange luminescence, and Fe^{2+} that quenches luminescence (Hemming et al., 1989; Machel and Burton, 1991). Presences of these elements are related to the changes of redox condition and pH of the pore fluids, causing different luminescence color (Wright and Tucker, 1990; Machel and Burton, 1991). Vadose zone is generally well oxygenated, which causes the Mn- and Fe-oxides to be absorbed onto other mineral surfaces causing low Mn^{2+} and Fe^{2+} content in pore fluids. Phreatic zone is in a reducing environment and pore fluids contain high Mn^{2+} content (Morad, 1998). Thus, carbonate formed in vadose zone has low luminescence intensity, while carbonate precipitated in phreatic zone displays brighter luminescence (Hemming et al., 1989; Machel and Burton, 1991). Variations of luminescence could be attributed to water table fluctuation causing carbonate precipitation varying between vadose and phreatic zones (Wright and Tucker, 1990; Machel and Burton, 1991), or the periodic

influx of waters from phreatic zone into the sediments of vadose zone (Marad, 1998).

Because the calcite cement in the White River Formation was predominantly formed during early diagenesis, the T(Δ_{47}) and calculated water $\delta^{18}O$ values should primarily reflect near-surface temperature and water isotope composition during deposition. The near-surface water also is not evaporated because evaporation tends to increase surface water Sr/Ca and Mg/Ca ratios. Davis et al. (2008) reported that evaporated early Eocene lake water in the Greater Green River Basin have Sr/Ca ratios of ~0.4 to 5 mmol/mol, which are significantly higher than the ratios in the White River Formation. The Sr/Ca and Mg/Ca ratios of the studied carbonate cement are consistently low before and after EOT, suggesting the cements were deposited in fresh water and the water chemistry remained unchanged across the EOT.

4.2 Small Changes of Paleoclimate and Paleoenvironment across EOT

The stable and clumped isotope compositions of the samples from the White River Formation reflect paleoclimate and paleoenvironment in eastern Wyoming during the latest Eocene and early Oligocene. $\delta^{13}C_{org}$ values of terrestrial plants are determined by plant photosynthetic pathways and aridity (Ehleringer, 1988; Farquhar et al., 1989; Cerling and Quade, 1993). Plants can be grouped into three categories based on photosynthetic pathways, including C_3, C_4 and crassulacean acid metabolism (CAM) (Farquhar el al., 1989; Celing and Quade 1993, Ehleringer and Monson, 1993). Pure C_3 plants have $\delta^{13}C_{org}$ values varying between -21‰ and -37 ‰, with an average of -27 ‰, while pure C_4 plants have values varying between -9‰ and -21‰, with an average of -12 ‰, and CAM plants have intermediate values (Farquhar et al., 1989; Cerling and Quade 1993; Ehleringer and Monson, 1993). C_4 plants may present as early as the Oligocene (Fox and Koch, 2003; Kubien and Sage, 2004; Tipple and Pagani, 2007), but definitely became widespread by the late Miocene (Cerling et al., 1997). Because the study period

crosses the EOT, C_4 and CAM pathway should play a negligible role in influencing the organic carbon isotope compositions of the White River Formation.

Water stress due to aridity influences organic matter $\delta^{13}C_{org}$ values by substantially decrease net fractionation of atmospheric CO_2 during photosynthesis, and biomass formed under water-stressed conditions have higher $\delta^{13}C_{org}$ values (Farquhar el al., 1982; Farquhar el al., 1989; Passey et al., 2002; Sharp, 2007; Wang et al., 2008). The $\delta^{13}C_{org}$ values in the White River Formation have a mean of -27.3 ‰, which is similar to the average $\delta^{13}C_{org}$ value of modern C_3 plant. The $\delta^{13}C_{org}$ values in eastern Wyoming remained nearly stable suggesting there was no obvious change of aridity or humidity across the EOT.

The $\delta^{13}C_{org}$ values of samples processed using acid digestion method is more vairable than the $\delta^{13}C_{org}$ values of samples processed using acid fumigation method, which have been documented in other studies (Harris et al., 2001, Komada et al, 2008; Larson et al., 2008). It is argued that acid digestion method can cause loss of acid soluble organic carbon, which typically has lower $\delta^{13}C_{org}$ values (Harris et al., 2001, Larson et al., 2008). It is also argued that acid digestion method sometime causes enhanced loss of ^{13}C-enriched compounds, and decreases $\delta^{13}C_{org}$ values (Komada et al., 2008). Therefore, here I only discuss the $\delta^{13}C_{org}$ values of samples processed using acid fumigation method.

Unlike organic carbon isotope, carbonate $\delta^{13}C$ values are controlled by three carbon sources, including breakdown of organic carbon, dissolved atmospheric CO_2, and dissolution of carbonate bedrock (Dettman et al., 1999). Organic carbons have mean $\delta^{13}C$ value of -27.3 ‰ based on results in this study. The $\delta^{13}C$ value of pre-industrial atmospheric CO_2 was -7 ‰, and was most likely stable during the Cenozoic (Sharp,

2007). In the study area, the bedrock that can be dissolved and influences surface water $\delta^{13}C$ values is the Paleozoic carbonate (Love and Christiansen, 1985), and there is no documented change of exhumation intensity across the EOT. The carbonate $\delta^{13}C$ values remained stable across the EOT, suggesting no changes of relative contributions of the three reservoirs across the EOT.

Ancient water $\delta^{18}O$ values provide insight regarding paleoclimate in the region. The carbonate cements were formed at shallow burial depth during early diagenesis, thus the water the carbonate precipitated from is most likely a mixture of groundwater and soil waters that are derived originally from precipitation. The $\delta^{18}O$ values of modern precipitation in eastern Wyoming vary between -13 ‰ and -8 ‰ annually, and the values of river water vary between -18 ‰ to -14 ‰ (Kendall and Coplen, 2001; Vachon et al., 2010). Our calculated water $\delta^{18}O$ values vary between -11.4‰ and -8.4 ‰, which are close to the values of precipitation, suggesting the water the carbonate cement precipitated from was mainly the local precipitation.

The change of T(Δ_{47}) values allows a maximum temperature decrease of 3 °C, which is the analytical uncertainty of clumped isotope thermometry. This amount is smaller than the documented temperature drop of ~8 °C in western Nebraska (Zanazzi et al., 2007) and ~10 °C in the United Kingdom (Hren et al., 2013). The carbonate $\delta^{18}O$ values increased ~0.5 ‰ across the EOT (Figure 3-5), which can be explained by a decrease of carbonate formation temperature of ~2.5°C if water $\delta^{18}O$ value did not change, or by an increase of water $\delta^{18}O$ value of ~0.5 ‰ if temperature did not change following Kim and O'Neil, (1997). Because surface cooling not only influences oxygen isotope fractionation between calcite and water, also causes a decrease in precipitation $\delta^{18}O$ values, ~2.5°C of cooling must be associated with a decrease in precipitation $\delta^{18}O$

values (Dansgaard, 1964), thus a net decrease in carbonate $\delta^{18}O$ values. This inference is opposite to our observation of increase in carbonate $\delta^{18}O$ values. Therefore, the increase of carbonate $\delta^{18}O$ values across the EOT is caused by changing water $\delta^{18}O$ values.

The latitude of the study area did not change and no dramatic tectonic deformation occurred in the study area and western U.S.A. across the EOT, ruling out changes of latitude, altitude and continentality as possible causes of changing water $\delta^{18}O$ values. The low and stable Sr/Ca and Mg/Ca ratios rule out evaporation as a cause of the increase of water $\delta^{18}O$ values. Here I suggest the increase of groundwater $\delta^{18}O$ values is resulted from gradual drying during the early Oligocene because $\delta^{18}O$ value of precipitation decreases ~2 ‰ when precipitation amount increases ~100 mm (Sharp, 2007). The ~0.5 ‰ increase in water $\delta^{18}O$ value can be caused by a ~25 mm decrease in precipitation amount. The early Eocene is generally wet because warm air masses hold more water vapor (Winguth et al., 2010, Carmichael el al., 2015). Cooler global climate after the EOT may decrease the amount of precipitation because cooler air masses hold less moisture. The drying may have influenced precipitation $\delta^{18}O$ values by sub-cloud evaporation (Bershaw et al., 2012). This drying was gradual based on the gradual change of water $\delta^{18}O$ values. The drying did not cause major ecology shift in the study area because the organic matter $\delta^{13}C$ values remained stable across the EOT.

My result of no major temperature change agrees with the results of paleosol geomorphology studies in Nebraska, Colorado, and South Dakota (Retallack et al., 1983; Terry et al., 2001; Retallack et al., 2007; Hembree and Hasiotis, 2007). My interpretation of no major paleoclimate change across the EOT is also consistent with the result of phytolith assemblage (Strömberg, 2004). The gradual drying after the EOT is consistent

with the change to eolian depositional environment in the White River Formation after the EOT (Evanoff, 1990), and concurrent drying in the central Rockies and western Nebraska based on volcanic glass hydrogen isotope studies (Fan et al., 2014). I suggest that the lack of dramatic climatic and environmental changes in eastern Wyoming in responses to global cooling across the EOT is a result of high topography in the central Rockies before the Oligocene. The central Rockies and the western Great Plains achieved their present high topography during the late Eocene (Fan et al., 2014). The cool climate in the high elevation region, similar to today's, may be less sensitive to global cooling (Fan et al., 2014).

4.3 Orbital Cycliciy

Climate changes often display cyclicity, and the cyclicity is attributed to oscillations in Earth's orbital parameters of precession, obliquity and eccentricity, which affect the amount and distribution of solar radiation the Earth receives. Precession cycles of 19 and 23 kyr influence annual and seasonal solar energy and is modulated by eccentricity. Obliquity cycles occur at 41 kyr and eccentricity at 100 kyr and 413 kyr. Previous study shows that the orbital periodicity of ~100 kyr have possibly paced the drastic cooling during the EOT (Zachos et al., 2001). Given the age gaps of most of my samples are ~40 kyr, it is not possible to document precession, obliquity, and shot eccentricity cyclicities. My data do not document the 400 kyr eccentricity cycles. However, power spectrum analysis of carbonate $\delta^{13}C$ and $\delta^{18}O$ values and calculated water $\delta^{18}O$ values show non-Milankovitch cycles of ~167 kyr above 95% confidence interval (Figure 3-6). The lack of Milankovitch cycles may be resulted from imprecise age determination by assuming stable sedimentation rates between dated ash beds.

Chapter 5

Conclusions

This study reconstructs paleoclimate and paleoenvironment across the Eocene-Oligocene boundary in the White River Formation in eastern Wyoming by integrating stable and clumped isotope values of carbonate cement and carbon isotope values of organic matter. The carbonate cements of the late Eocene-early Oligocene White River Formation are predominantly micritic low-magnesium calcite, with minor amount of spars filling vugs based on petrographic examinations and XRD analyses. These carbonate cements were formed in vadose and phreatic zones during early diagenesis, and their isotope compositions reflect near surface climate and environmental conditions in eastern Wyoming. Measured T(Δ_{47}) values show no substantial changes across the EOT. Although the analytical uncertainties of clumped isotope thermometry allows a maximum cooling of 3°C, cooler temperature predicts lower carbonate $\delta^{18}O$ values by influencing both precipitation $\delta^{18}O$ values and isotope fractionation, which is contrary to my observation of 0.5 ‰ increase in carbonate $\delta^{18}O$ values.

The 0.5 ‰ increase of carbonate cement $\delta^{18}O$ values and calculated water $\delta^{18}O$ values across the EOT suggest gradual drying due to cooler Oligocene global temperature and enhanced sub-cloud evaporation. The subtle drying did not cause environmental change for ecosystem because the organic matter $\delta^{13}C$ values remained stable across the EOT. Data provided in this study show that the North American continental interior did not experience dramatic changes in temperature and environment across the EOT as previously suggested. Subtle response to global cooling across the boundary in the central Rocky Mountains may be a result that high topography prior to the global cooling event buffered local responses to global cooling. Finally, spectrum analysis to isotope data in this study does not show that Milankovitch orbital cycles

modulate the paleoclimate in the central Rocky Mountains during the latest Oligocene-early Eocene.

Appendix A

Analysis Tables

Table A-1: Sr/Ca and Mg/Ca ratios of 11 samples analyzed by ICP-OES

Sample ID	Ca mg/L	Mg µg/L	Sr µg/L	Sr/Ca mmol/mol	Mg/Ca mol/mol
C-10EF-01	118	680	52	**0.203**	**0.010**
C-10EF-01	119	456	57	**0.220**	**0.006**
C-10EF-01 (avg)	119	568	55	**0.211**	**0.008**
C-10EF-15 blw ash	133	589	65	**0.222**	**0.007**
C-11EF-18	119	511	53	**0.203**	**0.007**
C-11EF-30	103	381	44	**0.195**	**0.006**
C-12EF-27	126	571	49	**0.177**	**0.007**
C-12EF-27	126	564	49	**0.176**	**0.007**
C-12EF-27	124	551	49	**0.180**	**0.007**
C-13EF-32	93	228	60	**0.294**	**0.004**
C-14EF-03	127	768	77	**0.279**	**0.010**
C-14EF-14	144	910	72	**0.229**	**0.010**
C-14EF-14	143	708	78	**0.249**	**0.008**
C-14EF-14 (avg)	144	809	75	**0.239**	**0.009**
C-15EF-23	110	281	63	**0.262**	**0.004**
C-15Ef-50	92	18	35	**0.171**	**0.000**
V-153F-90	53	198	36	**0.311**	**0.006**

Table A-2: Results of carbonate percentage, TOC, and isotope analysis

[a] SE is the standard error of D47, SE=SD(D47)/SQRT(N). When SD of a sample is less than the long-term SD of lab standard Carrara Marble, 0.013 is assigned as the SD of the sample when it is analyzed two times, and 0.011 is assigned as the SD of the sample whenit is analyzed three times.

[b] ARF=Absolute Reference Frame based on equation 6 in Defliese et al. (2015).

[c] Kim and O'Neil (1997): $10^3 \ln a = 18030/(T+273.15)-32.42$

Sample ID	Depth (m)	Age (Ma)	Carbonate (%)	TOC (%)	Δ47 (‰, HG) ARF	SE [a] (‰, HG) ARF	T (Δ47)[b] (°C)	$\delta^{13}C_{org}$ (‰, VPDB)	$\delta^{13}C$ (‰, VPDB)	$\delta^{18}O$ (‰, VPDB)	$\delta^{18}O_{water}$ [c] (‰, VSMOW)
After EOT											
15EF-90	215.5	32.25	28.6	0.05	0.708	0.011	22.1±4.8	-26.1	-6.7	-10.8	-9.0
15EF-90					0.69						
15EF-90					0.716						
15EF-83	208.5	32.36	42.3	0.03				-28.5	-6.0	-11.2	-9.0
15EF-62	182.5	32.77	31.7	0.09				-28.9	-6.4	-11.5	-9.3
15EF-56	181.5	32.79	13.9	0.21				-29.0			
15EF-50	175.5	32.88	41.7	0.03	0.724	0.008	19.2±5.2	-29.0	-5.9	-10.7	-9.5
15EF-50					0.702						
15EF-44	168.5	33.00	43	0.03					-6.6	-11.8	-9.6
2EF-top cong	170.5	32.96	4.2	0.05				-27.1			
2EF-top cong-4m	166.5	33.03	8.7	0.06				-27.0			
2EF-top cong-5m	165.5	33.04	9.5	0.05				-26.4			

Table A-2 – *Continued*

2EF-top cong-7m	163.5	33.08	35	0.03				-26.7	-5.9	-11.9	-9.8
15EF-30	154.5	33.22	36.5	0.04				-28.6	-6.9	-11.3	-9.1
15EF-23	147.5	33.33	47.8	0.04				-26.8	-5.8	-11.1	-9.0
15EF-20	144.5	33.38	29.4	0.04				-26.2	-6.5	-11.3	-9.1
15EF-14.5	139	33.47	55.9	0.05					-6.4	-11.0	-8.9
15EF-14	138.5	33.47	6.2	0.05							
15EF-12	136.5	33.51	7.2	0.05							
15EF-10m frac	134.5	33.54	6.6	0.05				-28.9			
15EF-7.5	132.3	33.57	43.5	0.03				-27.9	-6.5	-11.8	-9.6
15EF-7.5 teeth	132	33.58	62.8	0.05					-6.6	-12.1	-9.9
15EF-fossil near 7.5	131.5	33.59	48.5	0.03				-26.9	-7.7	-13.6	-11.4
15EF-04	128.5	33.63	46.5	0.03				-28.3	-6.1	-11.2	-9.0
2EF-51	136.5	33.51	11.3	0.07				-27.8			
2EF-47	132.5	33.57	49.1	0.03				-27.1	-5.8	-11.6	-9.4
2EF-44	129.5	33.62	5.6	0.04				-27.5			
2EF-41	126.5	33.67	45.5	0.05				-27.4	-5.6	-11.5	-9.3
14EF-6(c?)	127.5	33.65	51.3	0.03				-27.2	-6.3	-11.4	-9.2
2EF-39	124.5	33.70	55.7	0.04				-26.8	-5.3	-11.3	-9.2
14EF-22(6c)	127.5	33.65	5	0.04				-27.6			
2EF-6A ash	122.5	33.73	11.5	0.05				-27.6			
2EF-37(6A)	122	33.74	5.9	0.07				-27.6			
2EF-35	120.5	33.76	42.7	0.04				-27.0			

Table A-2 – *Continued*

2EF-32	117.5	33.81	60.5	0.04				-26.4	-5.4	-12.1	-9.9
14EF-16(6B)	121.5	33.74	10.2	0.04				-27.1	-6.8	-10.9	-8.8
2EF-30	120	33.77	6.2	0.05				-27.3			
14EF-14	119.5	33.78	53.8	0.04				-25.1	-6.3	-11.0	-8.8
2EF-28	117.5	33.81	55.8	0.04				-27.3	-5.4	-11.5	-9.3
14EF-12	117.5	33.81	57.3	0.06				-26.8	-6.1	-10.9	-8.8
2EF-25	114.5	33.86	53.9	0.05				-27.9	-8.3	-13.6	-11.4
14EF-10	115.5	33.84	52.8	0.05				-27.3	-6.0	-11.0	-8.9
14EF-08	113.5	33.87	60.2	0.05				-27.0	-6.6	-11.4	-9.2
14EF-06	111.5	33.90	48.4	0.04				-26.7	-7.3	-11.5	-9.3
2EF-20	119.5	33.78	7.4	0.08				-27.6			
2EF-19(5)	118.5	33.79	7.2	0.06				-27.6			
2EF-5(ash+2m)	107.5	33.97	8.3	0.07				-27.9			
2EF-18	117.5	33.81	14.6	0.21				-27.8			
14EF-03	108.5	33.95	52.7	0.04				-27.1	-5.7	-11.0	-8.9
EF2-04 snail			-	-	0.659	0.013	34.6±6.4		-7.2	-12.9	-8.7
EF2-04 snail			-	-	0.682				-7.0	-12.5	
Before EOT											
2EF-17v	116.5	33.82	11.3	0.11				-27.8			
2EF-17c	116	33.83	39.3	0.07					-6.7	-11.8	-9.7

Table A-2 – *Continued*

2EF-5(ash)	105.6	34.00	38.1	0.05				-26.9	-5.9	-12.8	-10.6
13EF-35(5)	105.5	34.00	8.5	0.04				-28.1			
2EF-5v(ash-2m)	103.5	34.02	8.8	0.08				-27.8			
2EF-5c(ash-2m)	103.5	34.02	48.4	0.1				-27.7	-5.5	-11.5	-9.3
13EF-32	102.5	34.03	44.7	0.03	0.703	0.006	26.1±4.9	-28.0	-5.7	-11.1	-8.5
13EF-32					0.684			-27.7			
2EF-05	92.5	34.11	8.4	0.1				-27.3	-5.7	-11.6	-9.4
2EF-5b	92	34.11	37.9	0.07				-26.9	-7.1	-12.5	-10.3
2EF-04	91.5	34.12	61	0.13				-26.9	-7.1	-12.5	-10.3
13EF-28	98.5	34.06	46.5	0.05				-27.4	-6.0	-10.8	-8.7
2EF-02 nod	90	34.13	45.2	0.04				-27.5	-5.5	-11.7	-9.5
2EF-02 matrix	89.7	34.13	7.8	0.06				-27.4			
2EF-02 smect	89.5	34.13	51.1	0.03				-26.3			
13EF-22	92.5	34.11	45.9	0.04				-27.1	-6.5	-11.0	-8.8
13EF-20	90.5	34.13	48.2	0.05				-27.1	-6.3	-11.0	-8.8
13EF-17	87.5	34.15	46.3	0.04				-27.5	-6.8	-12.3	-10.2
13EF-16	86.5	34.16	48.1	0.06				-27.4	-7.1	-11.7	-9.6
13EF-12	82.5	34.19	48.9	0.03				-26.3	-6.5	-11.5	-9.3
13EF-9	79.5	34.22	59.2	0.03				-26.8	-6.6	-11.5	-9.3
12EF-43 Ash 4	70.5	34.29	11.2	0.04				-26.6			
13EF-03	73.5	34.27	7.7	0.04				-27.7			
12EF-21(3c)	48.5	34.43	7.2	0.06				-26.5			

Table A-2 – *Continued*

12EF-27	54.5	34.48	53.7	0.03	0.675	0.012	30.1±3.9		-6.6	-11.8	-8.4
12EF-27					0.677						
12EF-27					0.694						
11EF-32	44.6	34.51	37.5	0.04				-27.2			
11EF-32 (3b)	44.5	34.51	10.8	0.04				-27.8			
12EF-16	43.5	34.52	51	0.05				-27.8	-6.9	-11.8	-9.6
12EF-16-3B	43	34.53	24.8	0.02				-27.7			
12EF-16 2nd carb	43.5	34.52	8.7	0.04				-27.5			
11EF-30	42.5	34.53	47.2	0.05				-27.3	-6.7	-11.9	-9.7
12EF-14	41.5	34.54	50.2	0.03					-6.6	-11.7	-9.5
12EF-12	40	34.55	62.3	0.02				-26.4	-6.9	-11.6	-9.4
11EF-27	39.5	34.56	50.5	0.03				-27.5	-6.8	-12.1	-10.0
12EF-10(3a)	37.6	34.57	42.7	0.05				-27.0	-8.2	-13.6	-11.4
11EF-25(3a ash)	37.5	34.57	10.8	0.04				-27.8			
11EF-24	36.5	34.58	51.7	0.04				-26.6	-6.6	-11.9	-9.7
12EF-07	34.5	34.60	50.3	0.03				-27.2	-7.3	-12.7	-10.6
11EF-21	33.5	34.61	49.5	0.05				-26.9	-6.8	-12.3	-10.1
11EF-18	30.5	34.63	52.3	0.06				-27.3	-6.8	-11.9	-9.8
12EF-01	28.5	34.65	7.1	0.02				-27.2			
11EF-15	27.5	34.66	53.5	0.05				-27.2	-6.9	-12.5	-10.3
11EF-12	24.5	34.68	58.5	0.03				-26.0	-7.0	-11.9	-9.8
11EF-10	22.5	34.70	-	-				-26.8	-6.9	-11.9	-9.8

Table A-2 – *Continued*

10EF-20(ash #2)	20	34.72	10.6	0.03				-27.9			
11EF-4	16.5	34.75	49	0.04				-26.7	-6.3	-11.8	-9.6
10EF-15 blw ash 2	15	34.76	49.5	0.05				-25.3	-6.2	-12.4	-10.2
11EF-1	14	34.77	58.5	0.04				-27.1	-6.4	-11.7	-9.5
10EF-13.5	13.5	34.77	53.9	0.03					-6.5	-12.1	-9.9
10EF-7.5	7.5	34.83	54.2	0.04				-27.4	-6.3	-12.1	-9.9
10EF-6	6	34.84	57.3	0.04				-27.3	-6.2	-11.9	-9.8
10EF-05 Ash1	5	34.85	9.5	0.11				-27.4			
10EF-04	4	34.85	50.5	0.03	0.709	0.013	22.8±3.6	-27.8	-6.4	-12.0	-10.1
10EF-04					0.695						
10EF-01	1	34.88	50.3	0.02				-27.6	-6.5	-11.3	-9.2
10EF-roots	0	34.89	31.19	0.03				-26.9			

Appendix B

Stable Isotope Equations

Delta notation is expressed as: **Eq.1**

$$\delta^{18}O\ (‰\ ,\ per\ mil) = \left(\left(^{18}O/^{16}O\right)_{sample} / \left(^{18}O/^{16}O\right)_{standard} - 1 \right) \times 1000$$

the standard is VPDB for carbonate, and VSMOW for water.

Fractionation factor is expressed as: **Eq. 2**

$$\alpha_{\ water\text{-}carbonate} = (1000 + \delta^{18}O_{\ water}) / (1000 + \delta^{18}O_{\ carbonate})$$

Following Kim and O'Neil, 1997, temperature dependence of equilibrium fractionation between calcite and water is expressed as: **Eq. 3**

$$1000 \ln\alpha(calcite\text{-}H_2O) = 18.03(10^3 T^{-1}) - 32.42$$

Δ_{47} notation is expressed as: **Eq. 4**

$$\Delta_{47}\ (‰\ ,\ per\ mil\ ) = \left((47/44)_{\ sample} / (47/44)_{\ stochastic} - 1 \right) \times 1000$$

Following Defliese et al. (2015), temperature is calculated from Δ_{47} using temperature is in Kelvin. **Eq.5**

$$\Delta_{47} = (0.03712 \times 10^6 / T^2) + 0.2784$$

References

Abels, H. A., Dupont-Nivet, G., Xiao, G., Bosboom, R., & Krijgsman, W., 2011. Step-wise change of Asian interior climate preceding the Eocene–Oligocene Transition (EOT). Palaeogeography, Palaeoclimatology, Palaeoecology, 299, 399-412.

Aubry, M. P., & Bord, D., 2009. Reshuffling the cards in the photic zone at the Eocene/Oligocene boundary. Geological Society of America Special Papers, 452, 279-301.

Augé, M., & Smith, R., 2009. An assemblage of early Oligocene lizards (Squamata) from the locality of Boutersem (Belgium), with comments on the Eocene–Oligocene transition. Zoological Journal of the Linnean Society, 155, 148-170.

Beckner, J. R., & Mozley, P. S., 1998, Origin and spatial distribution of early vadose and phreatic calcite cements in the Zia Formation, Albuquerque Basin, New Mexico, USA, in Morad, S. ed., Carbonate Cementation in Sandstones: International Association of Sedimentologists, Special Publication 26, pp. 27–52.

Bershaw, J., Penny, S.M., Garzione, C.N., 2012. Stable isotopes of modern water across the Himalaya and eastern Tibetan Plateau: Implications for estimates of paleoelevation and paleoclimate. J. Geophys. Res., Atmos. 117, D02110. http://dx.doi.org/10.1029/2011JD016132.

Bird, P., 1988. Formation of the Rocky Mountains, western United States: A continuum computer model. Science 239, 1501-1507.

Boardman, G.S., Secord, R., 2013. Stable isotope paleoecology of White River ungulates during the Eocene-Oligocene climate transition in northwestern Nebraska. Palaeogeography, Palaeoclimatology, Palaeoecology 375, 38-49.

Boardman, G. S., & Secord, R. (2013). Stable isotope paleoecology of White River ungulates during the Eocene–Oligocene climate transition in northwestern Nebraska. Palaeogeography, Palaeoclimatology, Palaeoecology, 375, 38-49.

Broecker, W. S., & Sanyal, A. (1998). Does atmospheric CO2 police the rate of chemical weathering?. Global Biogeochemical Cycles, 12(3), 403-408.

Bryson, R. A., Hare, F. K., 1974, The climates of North America, in: Bryson, R. A., Hare, F. K. (eds.), Climates of North America (world survey of climatology, v. 11), Elsevier, New York, pp.1-47.

Carmichael, M. J., Lunt, D. J., Huber, M., Heinemann, M., Kiehl, J., LeGrande, A., Loptson, C. A., Roberts, C.D., Sagoo, N., Shields, C., Valdes, P. J., Winguth, A., Winguth, C., Pancost, R. D., 2015. Insights into the early Eocene hydrological cycle from an ensemble of atmosphere-ocean GCM simulations. Climate of the Past Discussions 11, 3277-3339.

Cather, S. M., Connell, S. D., Chamberlin, R. M., McIntosh, W. C., Jones, G. E., Potochnik, A. R., ... & Johnson, P. S., 2008. The Chuska erg: Paleogeomorphic and paleoclimatic implications of an Oligocene sand sea on the Colorado Plateau. Geological Society of America Bulletin 120, 13-33.

Cather, S. M., Chapin, C. E., & Kelley, S. A., 2012. Diachronous episodes of Cenozoic erosion in southwestern North America and their relationship to surface uplift, paleoclimate, paleodrainage, and paleoaltimetry. Geosphere 8, 1177-1206.

Cerling, T. E., & Quade, J., 1993. Stable carbon and oxygen isotopes in soil carbonates. Geophysical Monograph Series 78, 217-231.

Cerling, T. E., Harris, J. M., MacFadden, B. J., Leakey, M. G., Quade, J., Eisenmann, V., & Ehleringer, J. R., 1997. Global vegetation change through the Miocene/Pliocene boundary. Nature 389, 153-158.

Coxall, H. K., Wilson, P. A., Pälike, H., Lear, C. H., & Backman, J., 2005. Rapid stepwise onset of Antarctic glaciation and deeper calcite compensation in the Pacific Ocean. Nature 433, 53-57.

Dansgaard, W., 1964. Stable isotopes in precipitation. Tellus A 16, 436-468.

Davis, S. J., Wiegand, B. A., Carroll, A. R., & Chamberlain, C. P., 2008. The effect of drainage reorganization on paleoaltimetry studies: An example from the Paleogene Laramide foreland. Earth and Planetary Science Letters 275, 258-268.

DeConto, R. M., & Pollard, D., 2003. Rapid Cenozoic glaciation of Antarctica induced by declining atmospheric CO2. Nature 421, 245-249.

Defliese, W.F., Hren, M.T., and Lohmann, K.C., 2015, Compositional and temperature effects of phosphoric acid fractionation on Δ47 analysis and implications for discrepant calibrations. Chemical Geology, 396, 51–60.

Dennis, K. J., Affek, H. P., Passey, B. H., Schrag, D. P., & Eiler, J. M., 2011. Defining an absolute reference frame for 'clumped'isotope studies of CO 2. Geochimica et Cosmochimica Acta 75, 7117-7131.

Dettman, D. L., Reische, A. K., & Lohmann, K. C., 1999. Controls on the stable isotope composition of seasonal growth bands in aragonitic fresh-water bivalves (Unionidae). Geochimica et Cosmochimica Acta 63, 1049-1057.

Dickinson, W.R., Klute, M.A., Hayes, M.J., Janecke, S.U., Lundin, E.R., McKittrick, M.A., & Olivares, M.D., 1988. Paleogeographic and paleotectonic setting of Laramide sedimentary basins in the central Rocky Mountain region. Geological Society of America Bulletin 100, 1023-1039.

Diester-Haass, L., & Zahn, R., 1996. Eocene-Oligocene transition in the Southern Ocean: History of water mass circulation and biological productivity. Geology 24, 163-166.

Dorothee., 2014 RedNoise_ConfidenceLevels. Matlab code. (http://www.mathworks.com/matlabcentral/fileexchange/45539-rednoise-confidencelevels/content/RedNoise_ConfidenceLevels/RedConf.m)

Dunkley Jones, T., Bown, P. R., Pearson, P. N., Wade, B. S., Coxall, H. K., & Lear, C. H. (2008). Major shifts in calcareous phytoplankton assemblages through the Eocene- Oligocene transition of Tanzania and their implications for low- latitude primary production. Paleoceanography 23, PA4204. doi:10.1029/2008PA001640.

Dupont-Nivet, G., Hoorn, C., & Konert, M., 2008. Tibetan uplift prior to the Eocene Oligocene climate transition: Evidence from pollen analysis of the Xining Basin. Geology 36, 987-990.

Ehleringer, J. R., & Monson, R. K., 1993. Evolutionary and ecological aspects of photosynthetic pathway variation. Annual Review of Ecology and Systematics 24, 411-439.

Ehleringer, J. R., 1989. Carbon isotope ratios and physiological processes in aridland plants: In Stable isotopes in ecological research. Springer, New York, pp 41-54.

Eldrett, J. S., Greenwood, D. R., Harding, I. C., & Huber, M., 2009. Increased seasonality through the Eocene to Oligocene transition in northern high latitudes. Nature 459, 969-973.

Evanoff, E., 1990. Late Eocene and early Oligocene paleoclimates as indicated by the sedimentology and nonmarine gastropods of the White River Formation near Douglas, Wyoming (Doctoral dissertation, University of Colorado).

Evanoff, E., Prothero, D. R., & Lander, R. H., 1992. Eocene-Oligocene climatic change in North America: the White River formation near Douglas, east-central Wyoming. Eocene-Oligocene Biotic and Climatic Evolution. Princeton University Press, Princeton, New Jersey, pp. 116-130.

Fan, M., Hough, B. G., & Passey, B. H., 2014. Middle to late Cenozoic cooling and high topography in the central Rocky Mountains: Constraints from clumped isotope geochemistry. Earth and Planetary Science Letters 408, 35-47.

Fox, D. L., & Koch, P. L., 2003. Tertiary history of C4 biomass in the Great Plains, USA. Geology 31, 809-812.

Farquhar, G. D., O'leary, M. H., & Berry, J. A., 1982. On the relationship between carbon isotope discrimination and the intercellular carbon dioxide concentration in leaves. Functional Plant Biology 9, 121-137.

Farquhar, G. D., Ehleringer, J. R., & Hubick, K. T., 1989. Carbon isotope discrimination and photosynthesis. Annual review of plant biology 40, 503-537.

Ghosh, P., Adkins, J., Affek, H., Balta, B., Guo, W., Schauble, E.A., Schrag, D. and Eiler, J.M., 2006. 13 C–18 O bonds in carbonate minerals: A new kind of paleothermometer. Geochimica et Cosmochimica Acta 70, 1439-1456.

Grimes, S. T., Hooker, J. J., Collinson, M. E., & Mattey, D. P., 2005. Summer temperatures of late Eocene to early Oligocene freshwaters. Geology 33, 189-192.

Goldner, A., Herold, N., & Huber, M., 2014. Antarctic glaciation caused ocean circulation changes at the Eocene-Oligocene transition. Nature 511, 574-577.

Harris, D., Horwáth, W. R., & van Kessel, C., 2001. Acid fumigation of soils to remove carbonates prior to total organic carbon or carbon-13 isotopic analysis. Soil Science Society of America Journal 65, 1853-1856.

Harris, W. G., Fisher, M. M., Cao, X., Osborne, T., & Ellis, L., 2007. Magnesium-rich minerals in sediment and suspended particulates of South Florida water bodies: implications for turbidity. Journal of Environmental Quality, 36, 1670-1677.

Hembree, D. I., & Hasiotis, S. T., 2007. Paleosols and ichnofossils of the White River Formation of Colorado: Insight into soil ecosystems of the North American Midcontinent during the Eocene-Oligocene transition. Palaios, 22, 123-142.

Hemming, N. G., Meyers, W. J., & Grams, J. C., 1989. Cathodoluminescence in diagenetic calcites: the roles of Fe and Mn as deduced from electron probe and spectrophotometric measurements. Journal of Sedimentary Research 59, 404-411.

Hren, M. T., Sheldon, N. D., Grimes, S. T., Collinson, M. E., Hooker, J. J., Bugler, M., & Lohmann, K. C., 2013. Terrestrial cooling in Northern Europe during the Eocene–Oligocene transition. Proceedings of the National Academy of Sciences 110, 7562-7567.

Ingraham, N. L., & Taylor, B. E., 1991. Light Stable Isotope Systematics of Large-Scale Hydrologic. Water Resources Research 27, 77-90.

Ivany, L. C., Lohmann, K. C., Hasiuk, F., Blake, D. B., Glass, A., Aronson, R. B., & Moody, R. M., 2008. Eocene climate record of a high southern latitude continental shelf: Seymour Island, Antarctica. Geological Society of America Bulletin 120, 659-678.

Keigwin, L. D., 1980. Palaeoceanographic change in the Pacific at the Eocene Oligocene boundary. Nature 287, 722-725.

Kim, S. T., & O'Neil, J. R., 1997. Equilibrium and nonequilibrium oxygen isotope effects in synthetic carbonates. Geochimica et Cosmochimica Acta 61, 3461-3475.

Kendall, C., & Coplen, T. B., 2001. Distribution of oxygen-18 and deuterium in river waters across the United States. Hydrological Processes 15, 1363-1393.

Kennett, J. P., 1977. Cenozoic evolution of Antarctic glaciation, the circum-Antarctic Ocean, and their impact on global paleoceanography. Journal of geophysical research, 82, 3843-3860.

Kohn, M. J., Josef, J. A., Madden, R., Kay, R., Vucetich, G., & Carlini, A. A., 2004. Climate stability across the Eocene-Oligocene transition, southern Argentina. Geology 32, 621-624.

Komada, T., Anderson, M. R., & Dorfmeier, C. L., 2008. Carbonate removal from coastal sediments for the determination of organic carbon and its isotopic signatures, δ13C and Δ14C: comparison of fumigation and direct acidification by hydrochloric acid. Limnology and Oceanography: Methods *6*, 254-262.

Kraatz, B. P., & Geisler, J. H., 2010. Eocene–Oligocene transition in Central Asia and its effects on mammalian evolution. Geology 38, 111-114.

Kubien, D. S., & Sage, R. F., 2004. Low-temperature photosynthetic performance of a C4 grass and a co-occurring C3 grass native to high latitudes. Plant, Cell & Environment 27, 907-916.

Larson, T. E., Heikoop, J. M., Perkins, G., Chipera, S. J., & Hess, M. A., 2008. Pretreatment technique for siderite removal for organic carbon isotope and C: N ratio analysis in geological samples. Rapid Communications in Mass Spectrometry 22, 865-872.

Lear, C. H., Elderfield, H., & Wilson, P. A., 2000. Cenozoic deep-sea temperatures and global ice volumes from Mg/Ca in benthic foraminiferal calcite. Science 287, 269-272.

Lear, C. H., Bailey, T. R., Pearson, P. N., Coxall, H. K., & Rosenthal, Y., 2008. Cooling and ice growth across the Eocene-Oligocene transition. Geology 36, 251-254.

Lipman, P. W., Prostka, H. J., & Christiansen, R. L., 1972. Cenozoic volcanism and plate-tectonic evolution of the western United States. I. Early and Middle Cenozoic. Philosophical Transactions of the Royal Society of London. Series A, Mathematical and Physical Sciences 271, 217-248.

Liu, Z., Pagani, M., Zinniker, D., DeConto, R., Huber, M., Brinkhuis, H., & Pearson, A., 2009. Global cooling during the Eocene-Oligocene climate transition. Science 323, 1187-1190.

Liu, Z., Bowen, G. J., Welker, J. M., 2010. Atmospheric circulation is reflected in precipitation isotope gradients over the conterminous United States. Journal of Geophysical Research 115, D22120. http://dx.doi.org/10.1029/2010JD014175.

Love, J.D, & Christiansen, A.C., 1985. Geological map of Wyoming. U.S. Geological Survey, scale 1:500,000, http://pubs.er.usgs.gov/publication/70046739.

Machel, H.G. & Burton, E.A., 1991. Factors governing cathodoluminescence in calcite and dolomite and their implication for studies of carbonate diagenesis, In: Barker CE, Kopp OC (eds) Luminescence microscopy quantitative and qualitative aspects. SEPM Short Course 25, 37–57

Mikolajewicz, U., Maier-Reimer, E., Crowley, T. J., & Kim, K. Y., 1993. Effect of Drake and Panamanian gateways on the circulation of an ocean model. Paleoceanography 8, 409-426.

Morad, S., Ismail, H. B., Ros, L. D., ALAASM, I. S., & SERRHINI, N. E., 1994. Diagenesis and formation water chemistry of Triassic reservoir sandstones from southern Tunisia. Sedimentology 41, 1253-1272.

Morad, S., 1998. Carbonate cementation in sandstones: distribution patterns and geochemical evolution, in: Morad, S., (ed.), Carbonate cementation in Sandstone, Blackwell Science, pp.1-26.

Obradovich, J. D., Evanoff, E., & Larson, E. E., 1995. Revised single-crystal laser-fusion 40Ar/39Ar ages of Chadronian tuffs in the White River Formation of Wyoming. In Geological Society of America Abstracts with Programs 3, A77.

Passey, B. H., Cerling, T. E., Perkins, M. E., Voorhies, M. R., Harris, J. M., & Tucker, S. T., 2002. Environmental change in the Great Plains: an isotopic record from fossil horses. The Journal of Geology 110, 123-140.

Passey, B. H., Levin, N. E., Cerling, T. E., Brown, F. H., & Eiler, J. M., 2010. High-temperature environments of human evolution in East Africa based on bond ordering in paleosol carbonates. Proceedings of the National Academy of Sciences 107, 11245-11249.

Pearson, P. N., Foster, G. L., & Wade, B. S., 2009. Atmospheric carbon dioxide through the Eocene–Oligocene climate transition. Nature 461, 1110-1113.

Prothero, D. R., 1995. Geochronology and Magnetostratigrapy of Paleocene North American Land Mammal.

Prothero, D. R., & Whittlesey, K. E., 1998. Magnetic stratigraphy and biostratigraphy of the Orellan and Whitney an land-mammal" ages" in the White River Group. Depositional Environments, Lithostratigraphy, and Biostratigraphy of the White River and Ankaree Groups (Late Eocene to Early Miocene North America). Geological Society of America Special Paper 325, 39-61.

Raymo, M. E., & Ruddiman, W. F., 1992. Tectonic forcing of late Cenozoic climate. Nature 359, 117-122.

Retallack, G. J., 1983. Late Eocene and Oligocene paleosols from Badlands National Park, South Dakota. Geological society of America.

Retallack, G. J., 2007. Cenozoic paleoclimate on land in North America. The Journal of Geology, 115, 271-294.

Schouten, S., Eldrett, J., Greenwood, D. R., Harding, I., Baas, M., & Damsté, J. S. S., 2008. Onset of long-term cooling of Greenland near the Eocene-Oligocene boundary as revealed by branched tetraether lipids. Geology 36, 147-150.

Sclater, J. G., & Christie, P., 1980. Continental stretching: An explanation of the post-mid-cretaceous subsidence of the central North Sea basin. Journal of Geophysical Research-Solid Earth 85, 3711-3739.

Scott, J,. (2000). High Precision U/Pb Geochronology of Oligocene Tuffs from the White River Formation, Douglas, Wyoming. SVP abstracts with programs, Journal of Vertebrate Paleontology 20, 69A.

Sharp, Z., 2007. Principles of stable isotope geochemistry. Upper Saddle River, New Jersey.

Sheldon, N. D., Costa, E., Cabrera, L., & Garcés, M., 2012. Continental climatic and weathering response to the Eocene-Oligocene transition. The Journal of Geology 120, 227-236.

Sijp, W. P., England, M. H., & Toggweiler, J. R., 2009. Effect of ocean gateway changes under greenhouse warmth. Journal of Climate 2, 6639-6652.

Squires, R. L., 2003. Turnovers in marine gastropod faunas during the Eocene-Oligocene transition, west coast of the United States in: From Greenhouse to Icehouse: The Marine Eocene–Oligocene Transition. Columbia University Press, New York, pp 14-35.

Strömberg, C. A., 2004. Using phytolith assemblages to reconstruct the origin and spread of grass-dominated habitats in the great plains of North America during the late Eocene to early Miocene. Palaeogeography, Palaeoclimatology, Palaeoecology 207, 239-275.

Swisher III, C. C., & Prothero, D. R., 1990. Single-crystal 40Ar/39Ar dating of the Eocene-Oligocene transition in North America. Science 249, 760-762.

Tipple, B. J., & Pagani, M., 2007. The early origins of terrestrial C4 photosynthesis. Annu. Rev. Earth Planet. Sci. 35, 435-461.

Terry Jr, D. O., 2001. Paleopedology of the Chadron Formation of Northwestern Nebraska: implications for paleoclimatic change in the North American midcontinent across the Eocene–Oligocene boundary. Palaeogeography, Palaeoclimatology, Palaeoecology 168, 1-38.

Vachon, R.W., Welker, J., White, J., Vaughn, B.H., 2010, Monthly precipitation isoscapes (δ18O) of the United States: Connections with surface temperatures, moisture source conditions, and air mass trajectories. Journal of Geophysical Research115, D21126, Doi: 10.1029/2010JD014105.

Van Andel, T. H., & Moore, T. C., 1974. Cenozoic calcium carbonate distribution and calcite compensation depth in the central equatorial Pacific Ocean. Geology 2, 87-92.

Van Andel, T. H., 1975. Mesozoic/Cenozoic calcite compensation depth and the global distribution of calcareous sediments. Earth and Planetary Science Letters 26, 187-194.

VanDeVelde, J. H., Bowen, G. J., Passey, B. H., & Bowen, B. B., 2013. Climatic and diagenetic signals in the stable isotope geochemistry of dolomitic paleosols

spanning the Paleocene–Eocene boundary. Geochimica et Cosmochimica Acta 109, 254-267.

Wade, Bridget S., Alexander JP Houben, Willemijn Quaijtaal, Stefan Schouten, Yair Rosenthal, Kenneth G. Miller, Miriam E. Katz, James D. Wright, and Henk Brinkhuis., 2012. Multiproxy record of abrupt sea-surface cooling across the Eocene-Oligocene transition in the Gulf of Mexico. Geology 40, 159-162.

Wang, G., Feng, X., Han, J., Zhou, L., Tan, W., & Su, F., 2008. Paleovegetation reconstruction using δ13 C of Soil Organic Matter. Biogeosciences Discussions 5, 1795-1823.

Whipkey, C. E., Capo, R. C., Hsieh, J. C., & Chadwick, O. A., 2002. Development of magnesian carbonates in Quaternary soils on the Island of Hawaii. Journal of Sedimentary Research 72, 158-165.

Winguth, A., Shellito, C., Shields, C., & Winguth, C., 2010. Climate response at the Paleocene-Eocene thermal maximum to greenhouse gas forcing-A model study with CCSM3. Journal of Climate 23, 2562-2584.

Wolfe, J.A., 1994. Tertiary climate changes at middle latitudes of western North America. Palaeogeography. Paleoclimatology. Palaeoecology 108, 195-205.

Worden, R. H., & Burley, S. D., 2003. Sandstone diagenesis: the evolution of sand to stone. Sandstone Diagenesis: Recent and Ancient, pp 1-44.

Wright, V.P., & Tucker, M.E., 1990, Carbonate Sedimentology, Blackwell Scientific Publication, 336-340.

Zachos, J. C., Quinn, T. M., & Salamy, K. A., 1996. High-resolution (104 years) deep-sea foraminiferal stable isotope records of the Eocene-Oligocene climate transition. Paleoceanography 11, 251-266.

Zachos, J., Pagani, M., Sloan, L., Thomas, E., Billups, K., 2001. Trends, rhythms, and aberrations in global climate 65 Ma to present. Science 292, 686-693.

Zachos, J. C., & Kump, L. R., 2005. Carbon cycle feedbacks and the initiation of Antarctic glaciation in the earliest Oligocene. Global and Planetary Change 47, 51-66.

Zanazzi, A., Kohn, M.J., McFadden, B.J., Terry Jr., D.O., 2007. Large temperature drop across the Eocene–Oligocene transition in central North America. Nature 445, 639–642.

Zanazzi, A., & Kohn, M. J., 2008. Ecology and physiology of White River mammals based on stable isotope ratios of teeth. Palaeogeography, Palaeoclimatology, Palaeoecology 257, 22-37.

Zhang, C., 2007. Fundamentals of environmental sampling and analysis. John Wiley & Sons Inc., Hoboken, New Jersey, pp 17.

Biographical Information

Sara Ayyash was born in January 5, 1992 in Abu Dhabi, UAE. She grew up there till the age of 6, and then moved to Texas, where she's lived most of her life. At a young age she had an interest in geology when she would collect rock off the playground and bring home. This eventually led to her perusing a Bachelor of Science in Geology with minor in Biology at the University of Texas at Arlington. She continued her education at UTA to pursue a Masters of Science in Environmental and Earth Science under the supervision of Dr. Majie Fan. She completed her Masters degree in December of 2015 and hopes to enter the job realm.